

## Multi-Objective Design of a Decentralized Structured $H_\infty$ -Based Controller for Longitudinal Helicopter Flight Dynamics

Capra, T.; Theodoulis, S.T.; Pavel, M.D.

**DOI**

[10.2514/6.2025-2244](https://doi.org/10.2514/6.2025-2244)

**Publication date**

2025

**Document Version**

Final published version

**Published in**

Proceedings of the AIAA SCITECH 2025 Forum

**Citation (APA)**

Capra, T., Theodoulis, S. T., & Pavel, M. D. (2025). Multi-Objective Design of a Decentralized Structured  $H_\infty$ -Based Controller for Longitudinal Helicopter Flight Dynamics. In *Proceedings of the AIAA SCITECH 2025 Forum* Article AIAA 2025-2244 (AIAA Science and Technology Forum and Exposition, AIAA SciTech Forum 2025). <https://doi.org/10.2514/6.2025-2244>

**Important note**

To cite this publication, please use the final published version (if applicable).  
Please check the document version above.

**Copyright**

Other than for strictly personal use, it is not permitted to download, forward or distribute the text or part of it, without the consent of the author(s) and/or copyright holder(s), unless the work is under an open content license such as Creative Commons.

**Takedown policy**

Please contact us and provide details if you believe this document breaches copyrights.  
We will remove access to the work immediately and investigate your claim.



# Multi-Objective Design of a Decentralized Structured $\mathcal{H}_\infty$ -based Controller for Longitudinal Helicopter Flight Dynamics

T. Capra <sup>\*</sup>, S. Theodoulis <sup>†</sup>, M.D. Pavel <sup>‡</sup>

*Delft University of Technology, P.O. Box 5058, 2600GB Delft, The Netherlands*

This paper introduces a multi-objective design approach for an Attitude Command-Attitude Hold (ACAH) and vertical velocity flight control system for the MBB Bo-105 helicopter longitudinal model. The design employs a decentralized structured  $\mathcal{H}_\infty$  dynamic controller using a PI-based and feed-forward control architecture, similar to the PID-based architecture commonly used in rotorcraft flight control design. The proposed design methodology integrates multi-objective approaches within the framework of structured  $\mathcal{H}_\infty$  control design. The uncertain model verifies the controller's performance under different flight configurations for a helicopter at 40 kts, using  $\mu$ -analysis which assesses robustness against model uncertainties. The multi-objective approach is employed in the control design process to tune parameters that balance handling qualities with robustness and stability. The performance of the resulting flight control system is investigated and evaluated against the required closed-loop time/frequency-domain criteria, as defined by ADS-33. The resulting design achieves Level 1 handling qualities, for which the advantages and limitations of the proposed methodology are discussed.

## I. Nomenclature

|   |   |
|---|---|
| $A, B, C$   | = state-space matrices  |
| $d_i, d_o$  | = disturbance input/output vector   |
| $e$   | = model following error signal  |
| $F_x$   | = body longitudinal $X$ component of the resultant force acting on the vehicle          |
| $F_z$   | = body normal $Z$ component of the resultant force acting on the vehicle                |
| $G$   | = linear helicopter model   |
| $H_{x,y}$   | = hard constraint performance with index $x, y$   |
| $I_{yy}$  | = pitch moment of inertia   |
| $K$   | = control system transfer functions, representing the controller dynamics in the system |
| $L, M$  | = real matrices characterising complex regions  |
| $m$   | = mass  |
| $M_u, M_w, M_q, M_\theta, M_{\delta_{col}}, M_{\delta_{lon}}$ | = moment derivatives normalized by moments of inertia                                   |
| $M_y$   | = body lateral $M$ component of the resultant moment acting on the vehicle              |
| $n$   | = measurement noise vector  |
| $q$   | = body rotational pitch rate  |
| $S_i, S_o$  | = input/output sensitivity function   |
| $S_{x,y}$   | = soft constraint performance with index $x, y$   |
| $T_i, T_o$  | = input/output complementary sensitivity function                                       |
| $T_{ref}$   | = reference model   |
| $T_{x \rightarrow y}$   | = transfer function from $x$ to $y$   |
| $u$   | = input vector  |
| $V_z$   | = helicopter body vertical velocity   |
| $W$   | = weighting filter  |
| $X_{CG}$  | = longitudinal center of gravity position   |
| $X_u, X_w, X_q, X_\theta, X_{\delta_{col}}, X_{\delta_{lon}}$ | = $X$ force derivatives normalized by helicopter mass                                   |

<sup>\*</sup>M.Sc., Faculty of Aerospace Engineering, Control and Simulation Division, Delft University of Technology

<sup>†</sup>Assoc. Professor, Faculty of Aerospace Engineering, Control and Simulation Division, Delft University of Technology, AIAA Assoc. Fellow

<sup>‡</sup>Assoc. Professor, Faculty of Aerospace Engineering, Control and Simulation Division, Delft University of Technology

|   |   |   |
|---|---|---|
| $y$   | = | measured output vector  |
| $Z_{CG}$  | = | vertical center of gravity position                           |
| $Z_u, Z_w, Z_q, Z_\theta, Z_{\delta_{col}}, Z_{\delta_{lon}}$ | = | $Z$ force derivatives normalized by helicopter mass           |
| $\zeta$   | = | damping ratio   |
| $\delta_{col}, \delta_{lon}$                                  | = | helicopter inputs: collective and longitudinal cyclic         |
| $\delta_{col,cmd}, \delta_{lon,cmd}$                          | = | actuator inputs: commanded collective and longitudinal cyclic |
| $\theta$  | = | helicopter attitude pitch                                     |
| $\omega_n$  | = | natural frequency   |

## II. Introduction

THE development of rotorcraft has been a long and challenging process involving simulation, analysis, and design iterations. Control systems and handling qualities have required significant attention from both designers and pilots. Due to the dynamic instability of rotorcraft during flight, artificial stability augmentation or a full authority flight control system is necessary to meet stability and handling requirements [1–3]. Developments such as fly-by-wire and electronic stabilization systems have improved rotorcraft handling qualities [4–6]. Several techniques have been investigated to address the challenges of controllability in rotorcraft [7].

Enhancing rotorcraft handling qualities (HQ) for desirable characteristics in the time/frequency domain is specified in guidelines such as ADS-33E-PRF [6] and stability characteristics in the MIL documents [8]. However, complex flow phenomena generated by rotor blades can significantly affect helicopter dynamics, such as irregular flows from vortex interaction and downwash caused by the main rotor on the tail surface [9]. The uncertainty in these unstable dynamics, particularly for agile helicopters, makes the development of flight control laws a serious technical challenge, limiting control system design solutions in terms of both handling quality performance and robustness against uncertainties.

In essence, there are many robust control methods that can account for system uncertainties by incorporating their worst-case conditions in the design phase, aiming to design a control system that remains stable with adequate stability margins and meets performance objectives [10]. The implementation of robust control for rotorcraft vehicles varies across studies in methodology, using multivariable robust control theories such as LQG/LTR,  $\mathcal{H}_\infty$ ,  $\mathcal{H}_2$ , etc., for control law tuning in [11–15], which are industry standards [10]. This is due to the advantages these methods offer, enabling trade-offs between performance, stability, and robustness through the optimization of weighted signal/transfer function norms. Recent studies have developed techniques aimed at either integrating handling requirements [16–18] or accounting for model uncertainty [13, 19] in control design for helicopter models. The most recent method accomplishing both [20, 21] using a 2-step optimization approach optimising model following structure and control attenuation in which the controller is robustified using a multi-model approach. Recent advances in non-smooth optimization techniques, where the non-convexity issue has been resolved and incorporated in MATLAB functions *sysune()* and *hinfstruct()*, allow for multi-modal/multi-objective control design [22]. By leveraging multivariable robust control theory through signal-based optimization, it is possible to achieve lower-order and simpler fixed-structure controllers optimized with multiple objectives for both HQ criteria and robustness against uncertainty, often approaching the robustness of unstructured/full-order controllers. However, controller order reduction often leads to a loss of robustness without specialized order reduction techniques, as demonstrated in [23–26].

In this paper, an Attitude Command-Attitude Hold (ACAH) and vertical velocity flight control system for the MBB Bo-105 helicopter is presented. The paper focuses exclusively on the longitudinal model, which was developed based on a multi-objective approach using closed-loop transfer functions to design for robustness [23, 27]. Reference models are employed in model-following methods to enforce HQ objectives, serving as a trade-off between performance and robustness. The helicopter model utilises the bare airframe dynamics of the Bo-105 helicopter, which entails steady-state longitudinal flapping and one-dimensional inflow dynamics with actuators. The control structure used is decentralized Proportional-Integral-like (PI-like) control with a feedforward control element. This structure combines feedback control for stability and robustness against model uncertainties with feedforward control to achieve the necessary HQ objectives. Additional design objectives were established in the form of  $\mathcal{H}_\infty$  constraints between the reference models and the actual system response, minimum disk-based stability margins, and minimization of disturbances at the input/output (I/O) to the control signal and measured output of the plant. The controller addresses flight speeds around 40 knots at sea level altitude. This approach uses robust control theory for the  $\mathcal{H}_\infty$  constraints combined with structured singular value (SSV) analysis to assess the robustness of the design against parametric uncertainties.

This paper is organized as follows. Section III introduces the helicopter model. Section IV details the closed-loop controller architectures and design methodology, describing the objectives implemented. Section V looks at the results and analysis of the performance of the resulting design in both the time and frequency domains. The conclusions are presented in Section VII.

### III. Bo105 Helicopter Model

The MBB Bo-105 longitudinal helicopter was selected due to its well-known dynamic instability, which poses challenges and limitations to robustness in the design of control laws. An analysis of the Bo-105 bare airframe dynamics [18, 28] shows that an unstable phugoid mode is present across the flight envelope. Additionally, there are local right-half-plane (RHP) zeros in the collective control channel ( $\delta_{col}$ ), with the presence of a transmission zero near the marginal stability plane at  $-0.015$  in all of the channels when linearizing, as shown in Fig. (1). This figure shows phugoid poles in the RHP at  $0.1 \pm 0.29i$ , as well as the heave and pitch subsidence in the stable left-half-plane at  $-0.43$  and  $-1.1$ , respectively. The existence of RHP poles imposes fundamental limitations because they introduce unstable open-loop behavior, which increases the difficulty of ensuring stability and robustness in the control system's design. Additionally, RHP poles and zeros restrict the controller's ability to simultaneously achieve high performance (e.g., fast tracking or disturbance rejection) and robustness against uncertainties, as these elements constrain achievable gain and phase margins.

The helicopter dynamics are represented in the design process by a linear time-invariant model, given by Eq. (1). Here,  $x = [u \ w \ q \ \theta]^T$  is the state vector and  $u = [\delta_{col} \ \delta_{lon}]^T$  is the control input. The vector  $u$  comprises the collective and longitudinal inputs, in that order.  $A$ ,  $B$ , and  $C$  are the stability, control, and output matrices, respectively. The measurement vector  $y$  comprises the measurements of the attitude angle  $\theta$ , body-axis angular velocity  $q$  and the vertical velocity  $V_z$ . The model used is an analytical model based on [29–31], which is reduced to only the longitudinal mode. These matrices represent the 3 degrees of freedom (DoF) rigid-body dynamics ( $u, w, q$ ) of the helicopter without the horizontal tail forces. The quasi-steady inflow of the main rotor is represented by a first-order model whose time constant is set to 0.1 s. This augmentation leads to a simplified 5th-order non-linear longitudinal helicopter model, which includes inflow dynamics to trim the thrust coefficient and steady-state longitudinal flapping. This model is solved to determine the operating equilibrium point, which satisfies the equilibrium condition ( $\dot{x} = f(x, u) = 0$ ) for straight and steady horizontal flight. Linearizing the model at these points provides the state-space matrices  $A$ ,  $B$  and  $C$  in Eq. (1), assuming the non-dimensional inflow remains constant. Finally, a second-order actuator dynamics model of the Bo-105 helicopter ( $\omega_n = 50 \text{ rad/s}, \zeta = 0.95$ ) described in [32] is augmented in each of the collective and longitudinal control channels.

$$G_{AF} : \quad \dot{x} = Ax + Bu \quad y = Cx \quad (1)$$

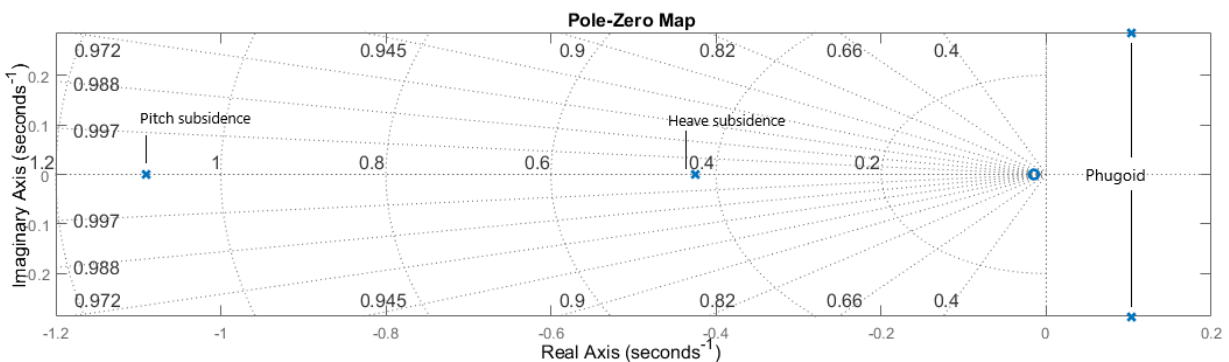


Fig. 1 Open-loop pole-zero plot of longitudinal bare-frame helicopter model at 40 kts

## IV. Flight Control Design

### A. Design Layout

The transfer function I/O relationships used for decentralized control design are shown in Fig. (2). The actuator model  $G_{act}$  consists of second-order transfer functions with  $\omega_n = 50$  rad/s and  $\zeta = 0.95$ , applied to both input channels [32]. The two-degrees-of-freedom controller has two outputs and five inputs, since it includes both the reference and the measured signals of the controlled variables: vertical velocity, pitch rate, and pitch, respectively  $V_z, q, \theta$ . The external signals are the disturbances at the input  $d_i$  composed of  $d_{\delta_{col,cmd}}, d_{\delta_{lon,cmd}}$  and at the output  $d_o$  composed of  $d_{V_z}, d_q, d_\theta$  as well as the sensor noise  $n$  composed of  $n_{V_z}, n_q, n_\theta$ . Other signals involved in the controller design are the reference tracking signals  $V_{zref}$  and  $\theta_{ref}$ , the disturbed outputs  $y$ , composed of the measurements for  $V_z, q, \theta$  and the actuator inputs, which are the commanded inputs  $u$  composed of  $\delta_{col,cmd}, \delta_{lon,cmd}$  as the controller outputs.

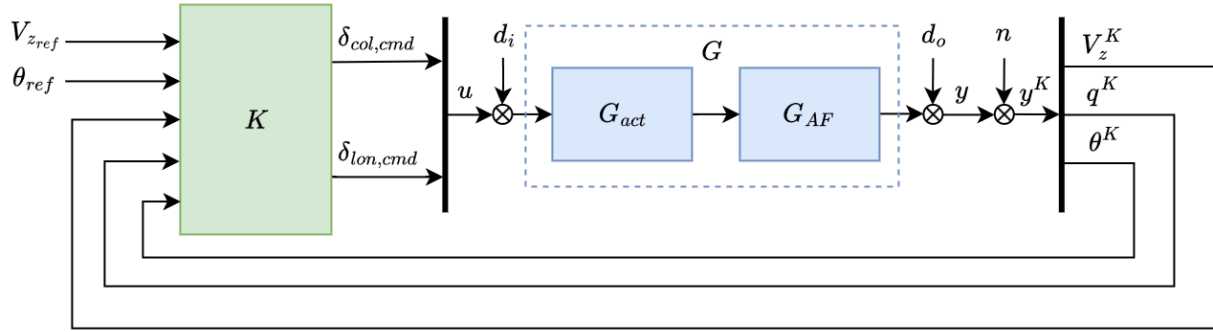


Fig. 2 Longitudinal helicopter controller I/O layout

### B. Control Layout

The autopilot structure used here is decentralized as shown Fig. (3). This structure, consist of three key components. Firstly, the feed-forward injection  $K_{inj}$  using a second-order transfer functions to adjust the input signal  $u$  based on the reference signals  $V_{zref}$  and  $\theta_{ref}$ . The structure of  $K_{inj,V_z}$  and  $K_{inj,\theta}$  is as follows:

$$K_{inj}(s) = \frac{z_1 s + z_0}{s^2 + p_1 s + p_0} \quad (2)$$

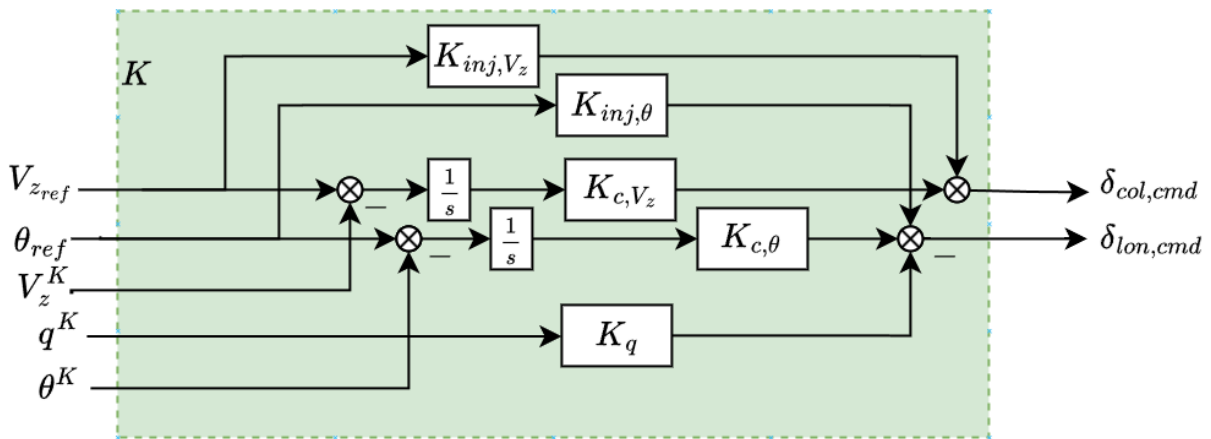


Fig. 3 Longitudinal helicopter control structure

The second components are the first-order transfer functions  $K_c$ , which act as a PI-like controllers though the integrator with a low-pass filter with frequency of  $\omega_c$ . This is used for tracking the reference signals  $V_{zref}$  and  $\theta_{ref}$  in the autopilot loop. The structure of  $K_{c,V_z}$  and  $K_{c,\theta}$  is as follows:

$$\frac{K_c(s)}{s} = \frac{K_p s + K_i}{s} \cdot \frac{\omega_c}{s + \omega_c} \quad (3)$$

Final component is the static output gain  $K_q$  which stabilizes the phugoid mode of the helicopter, improving the damping and transient response. The order of the tuned controller was determined after successive iterations in which the controller order of  $K_c$  and  $K_{inj}$  was increased incrementally. These iterations revealed that the performance of the controller increased with increased order until the robustness and handling qualities performance leveled off.

### C. Design Specifications

The flight control laws for robust control in the following sections are designed to fulfill a series of hard constraints which are bounded by  $\max H_{i,j} < 1$  and soft constraints which are optimised by minimising  $\max S_{i,j}$  using the signals in Fig. (2) for the specified design points. The hard constraints involve the minimum necessary stability at the I/O of the plant, broken-loop-at-a-time, and pole placement constraint [33]. The soft constraints involve various I/O disturbance rejection and control attenuation shown in Eq. (4) for the vertical velocity and attitude control. Furthermore, reference tracking for the vertical velocity and attitude control described in Eq. (5). The individual transfer functions are taken from Eq. (4) and Eq. (5) matrices, which are used to separately bound the vertical velocity and attitude control loops and optimize the robustness of the controller.

$$\begin{bmatrix} y \\ u \end{bmatrix} = \begin{bmatrix} S_o & S_o G \\ K S_o & T_i \end{bmatrix} \cdot \begin{bmatrix} d_o \\ d_i \end{bmatrix} \quad (4)$$

$$\begin{bmatrix} e_{V_z} \\ e_{\theta} \end{bmatrix} = (T_o - T_{ref}) \cdot \begin{bmatrix} V_{zref} \\ \theta_{ref} \end{bmatrix} \quad (5)$$

#### 1. Hard Constraints

For the stability margin requirement, minimum robust disk-based stability margins are applied at each of the actuator inputs  $u$  for commanded collective  $\delta_{col,cmd}$  and commanded longitudinal  $\delta_{lon,cmd}$ , and at each of the helicopter outputs  $y$  for vertical velocity  $V_z$ , pitch rate  $q$ , and pitch  $\theta$ , broken loop-at-a-time. The margins can be assessed by breaking the loop at set points in the control loop to guarantee robustness to simultaneous gain and phase variations, unlike classical gain and phase margins [34]. These constraints can be written in terms of the open-loop transfer functions  $L$  associated with each of the five channels computed at each input or outputs. To define the symmetric disk-based stability margins, the constraint for  $i^{th}$  input/output is written as:

$$H_{1,i} = \frac{\alpha_{max}}{2} \left\| \frac{I - L}{I + L} \right\|_{\infty} \leq 1 \quad (6)$$

Given the parameters  $\alpha_{max}$  which is the disk size for the guaranteed minimum gain  $[\gamma_{min}, \gamma_{max}]$  and phase margins  $[\phi_{min}, \phi_{max}]$  written as [34]:

$$[\gamma_{min}, \gamma_{max}] = \left[ \frac{2 - \alpha_{max}}{2 + \alpha_{max}}, \frac{2 + \alpha_{max}}{2 - \alpha_{max}} \right] \quad (7)$$

$$[\phi_{min}, \phi_{max}] = \left[ -\arccos \left( \frac{1 + \gamma_{min} \gamma_{max}}{\gamma_{min} + \gamma_{max}} \right), \arccos \left( \frac{1 + \gamma_{min} \gamma_{max}}{\gamma_{min} + \gamma_{max}} \right) \right] \quad (8)$$

The minimum required classical margins of  $\pm 6$  dB/ $\pm 45$  deg from a MIL document in [8] which are used as a standard for stability margins in flight control system design. With the minimum phase margins being the limiting parameter for the size of the disk  $\alpha_{max} = 0.82$  in systematic case which results in  $\pm 7.6$  dB/ $\pm 45$  deg for the constraint.

For the pole-placement requirement described in the HQ criteria for low speed flight and longitudinal modes, in terms of stability is a reasonable demand that the system's closed poles lie in a particular subset of the complex plane  $\mathcal{D}$  for the design point at 40 kts.

This guarantees certain criteria, such as sufficient damping and stable RHP-poles. The damping ratio is set to 0.35, with a minimum decay rate of 0, to meet HQ objectives defined using the ADS-33 criteria [6]. The maximum frequency of 100 rad/s for the poles is bounded in the region of the complex plane to avoid dynamics faster than the sampling rate, which is assumed to be 100 Hz. Here,  $L = L^T$  and  $M$  are real matrices that can characterize a variety of regions on the complex plane [35]. Such a region is defined as:

$$H_{2,1} : \mathcal{D} = \{z \in \mathbb{C} : f_{\mathcal{D}}(z) = L + zM + \bar{z}M^T < 0\} \quad (9)$$

## 2. Soft Constraints

The disturbance rejection requirements involve rejecting plant I/O disturbances toward the measured output. The output disturbance rejection is defined by the output sensitivity transfer function  $S_o$  from the output disturbance  $d_o$  to the measured output  $y$ . These constraints are established based on the analysis in [36] which uses HQ criteria and through experimentation establishing recommend guidelines for the output disturbance sensitivity. The disturbance rejection peak  $DRP$  and disturbance rejection bandwidth  $DRB$  are used to evaluate the handling and hold characteristics for each output channel. These parameters are defined as follows:

$$\omega(S_o = -3 \text{ dB}) = DRB \text{ rad/s}, \quad \|S_o\|_{\infty} = DRP \text{ dB} \quad (10)$$

The specifications on disturbance rejection are defined and enforced with the weighting function  $W_{S_o}$ . The transfer functions from  $T_{d_{V_z} \rightarrow V_z}$  and  $T_{d_{\theta} \rightarrow \theta}$  are subject to the required specifications for the vertical velocity and attitude channels, shown in Table 1 for the hold characteristics.

**Table 1 Disturbance rejection guidelines [36]**

|                          | Pitch ( $\theta$ ) | Vertical velocity ( $V_z$ ) |
|--------------------------|--------------------|-----------------------------|
| $DRB \text{ rad/s} \geq$ | 0.5                | 1.0                         |
| $DRP \text{ dB} \leq$    | 5.0                | 5.0                         |

The low-frequency gain must be reduced to reject disturbances in this range for the respective hold modes and to limit signal amplification. Therefore, the inverted weighting function  $W_{S_o}^{-1}$  is chosen such that the low-frequency attenuation converges to  $-40$  dB. The constraints are written as:

$$S_{1,1} = \|W_{S_{V_z}} T_{d_{V_z} \rightarrow V_z}\|_{\infty} \quad (11)$$

$$S_{1,2} = \|W_{S_{\theta}} T_{d_{\theta} \rightarrow \theta}\|_{\infty} \quad (12)$$

The input disturbance rejection is defined as  $S_o G$ , the transfer function from the input disturbance  $d_i$  to the measured output  $y$ . Similarly, control signal attenuation is defined as the transfer function from the output disturbance  $d_o$  to the control output  $u$ . To align the system's I/O relationships across different operating points, the system's plant can be re-scaled, allowing the functions  $S_o G$  and  $K S_o$  to be normalized. The re-scaling of the direct control (DC) gains in the open-loop system leads to specific results for the  $K S_o$  functions, ensuring that the transfer functions  $T_{d_{V_z} \rightarrow \delta_{col,cmd}}$  and  $T_{d_{\theta} \rightarrow \delta_{lon,cmd}}$  maintain a consistent value of 0 dB at a frequency of 0 rad/s, as mentioned in [23]. For input disturbance rejection, the re-scaling is inverted as the I/O relationships are reversed. Additionally, due to normalization, similar weights can be applied for the input and output disturbance rejection. Although, for  $W'_{S_{\theta}}$ , the roll-off is altered compared to  $W_{S_{\theta}}$  to match the slope of the re-scaled  $S_o G$  function. The constraints are written as:

$$S_{2,1} = \|W_{S_{V_z}} T_{d_{\delta_{col,cmd}} \rightarrow V_z}\|_{\infty} \quad (13)$$

$$S_{2,2} = \|W'_{S_{\theta}} T_{d_{\delta_{lon,cmd}} \rightarrow \theta}\|_{\infty} \quad (14)$$

For the control signal attenuation for the feedback loop is defined as  $K S_o$ , represented by  $T_{d_{V_z} \rightarrow \delta_{col,cmd}}$  and  $T_{d_{\theta} \rightarrow \delta_{lon,cmd}}$ , the inverted weighting filters are adjusted so that the transfer functions are bounded, limiting the peak values and high frequency gains. The low frequencies are limited by gains of 10 dB for both channels to provide robustness to output multiplicative uncertainty for output related the corresponding disturbance input.

With sufficient roll-off at frequencies of 10 rad/s and 20 rad/s for the control signal attenuation of the vertical velocity and attitude control channels, respectively. Furthermore, high-frequency gains are attenuated at  $-40$  dB in order to ensure reduced control effort at high frequencies limiting the effect of sensor noise on the controller. The following constraints are written as:

$$S_{3,1} = \left\| W_{KS_{V_z}} T_{d_{V_z} \rightarrow \delta_{col,cmd}} \right\|_{\infty} \quad (15)$$

$$S_{3,2} = \left\| W_{KS_{\theta}} T_{d_{\theta} \rightarrow \delta_{lon,cmd}} \right\|_{\infty} \quad (16)$$

The input tracking is defined as  $T_i$ , the transfer function from input disturbance  $d_i$  to the controller output  $u$ . These transfer functions, represented by  $T_{d_{\delta_{col,cmd}} \rightarrow \delta_{col,cmd}}$  and  $T_{d_{\delta_{lon,cmd}} \rightarrow \delta_{lon,cmd}}$ , are constrained to enforce low-frequency input open-loop crossover. The weighting functions limit the input tracking to provide robustness against uncertainties at the actuator input. For the weighting functions in the  $\delta_{col,cmd}$  channel are 3 rad/s and for the  $\delta_{lon,cmd}$  channel 15 rad/s are limited to 0 dB. With high-frequency gains of  $-40$  dB in order to ensure a good attenuation of control disturbances at high frequencies at the input. The following constraints are written as:

$$S_{4,1} = \left\| W_{T_{\delta_{col,cmd}}} T_{d_{\delta_{col,cmd}} \rightarrow \delta_{col,cmd}} \right\|_{\infty} \quad (17)$$

$$S_{4,2} = \left\| W_{T_{\delta_{lon,cmd}}} T_{d_{\delta_{lon,cmd}} \rightarrow \delta_{lon,cmd}} \right\|_{\infty} \quad (18)$$

The model following method is used to focus on time-domain transient responses. In which, a lower-order equivalent system (LOES) for the collective to height rate response from the HQ criteria is used to evaluate the vertical velocity response characteristics for desirable reference tracking performance, written as:

$$T_{ref,V_z} = \frac{K e^{-\tau_{V_{zeq}} s}}{T_{V_{zeq}} s + 1} \quad (19)$$

The parameters which relate directly to meet the level 1 HQ criteria for the LOES for vertical velocity response are shown in Table 2 using the model following structure.

**Table 2 Parameters for the model following of  $T_{ref,V_z}$**

| Parameter        | Description   | Value |
|------------------|---------------|-------|
| $\tau_{V_{zeq}}$ | Time delay    | 5 ms  |
| $T_{V_{zeq}}$    | Time constant | 1.0 s |

The pitch control (ACAH) has reference following requirements for rise time and closed-loop shaping for level 1 handling qualities for  $T_o$ , the signal for the reference tracking performance. The LOES is formulated based on approximations seen in [2], written as:

$$T_{ref,\theta} = \frac{\omega_n^2 e^{-\tau_{\theta_{eq}} s}}{s^2 + 2\zeta\omega_n s + \omega_n^2} \quad (20)$$

The parameters which meet the level 1 HQ criteria are described in Table 3 using the model following structure, where the quickness requirement is the limiting constraint and the delay bounds phase-lag in the closed-loop bandwidth of the handling requirements.

**Table 3 Parameters for the model following of  $T_{ref,\theta}$**

| Parameter            | Description       | Value     |
|----------------------|-------------------|-----------|
| $\tau_{\theta_{eq}}$ | Time delay        | 7.5 ms    |
| $\zeta$              | Damping ratio     | 1         |
| $\omega_n$           | Natural frequency | 4.5 rad/s |

The targeted HQ criteria for the phase delay  $\tau_{p\theta}$  is 0.05 s with a bandwidth  $\omega_{BW\theta}$  of 6.3 rad/s and the response speed  $\frac{q_{pk}}{\theta_{pk}}$  of  $1.6 s^{-1}$ .

The delay's for both channels can be linearized using a first-order approximation for the constraint. To ensure compliance with HQ criteria, low steady-state error is achieved through limiting the  $\mathcal{H}_\infty$  norm of the weighted reference error signal at low frequencies, bounding the transfer functions  $T_{V_{zref} \rightarrow V_z}$  and  $T_{\theta_{ref} \rightarrow \theta}$ . Furthermore, to ensure that the frequency domain response are followed at low to mid-frequencies, attenuation is required of  $-40$  dB at  $1$  rad/s applied to both channels with a roll-off relaxing the constraint at higher frequencies where matching is less critical. The following constraints are written as:

$$S_{5,1} = \left\| W_{T_{V_z}} (T_{V_{zref} \rightarrow V_z} - T_{ref,V_z}) \right\|_\infty \quad (21)$$

$$S_{5,2} = \left\| W_{T_\theta} (T_{\theta_{ref} \rightarrow \theta} - T_{ref,\theta}) \right\|_\infty \quad (22)$$

## V. Results & Analysis

The synthesized controller was obtained after tuning the five control gains  $K_{inj,V_z}$ ,  $K_{inj,\theta}$ ,  $K_{c,V_z}$ ,  $K_{c,\theta}$ ,  $K_q$  to meet the soft and hard design specifications described above. The solution was derived using the *systeme()* function in the MATLAB Control Design Toolbox, which handles multi-objective design problems [22, 37, 38]. In this approach, the soft design constraints  $S_{i,j}$  are minimized while ensuring that the hard constraints  $H_{i,j}$  are satisfied, as detailed in [21, 27]. Along with the controller gains, the function returns two scalar values:  $\max(H_{i,j}) = 1$  and  $\max(S_{i,j}) = 0.9$ , which verify whether the constraints are satisfied by the controller. The synthesized structured  $\mathcal{H}_\infty$  controller is expressed as follows:

$$\begin{aligned} K_{inj,V_z} &= \frac{0.056s - 0.30}{s^2 + 12.24s + 54.04} & K_{inj,\theta} &= \frac{-46.87s + 26.46}{s^2 + 11.36s + 46.16} \\ K_{c,V_z} &= \frac{0.064s + 0.066}{s + 5.45} & K_{c,\theta} &= \frac{-11.09s - 5.67}{s + 4.87} & K_q &= -1.97 \end{aligned} \quad (23)$$

### A. Stability Requirements

In Fig. (4) and (5), the disk-based gain and phase margins as functions of frequency are shown for each of the helicopter inputs and outputs. The minimum classical gain margins are approximately  $\pm 12$  dB or greater for all inputs and outputs, which is well above the 6 dB objective. In contrast, the minimum classical phase margins are  $\pm 45$  deg or greater that are on target, as the hard constraint only guarantees  $\pm 7.6$  dB and  $\pm 45$  deg of classical margins.

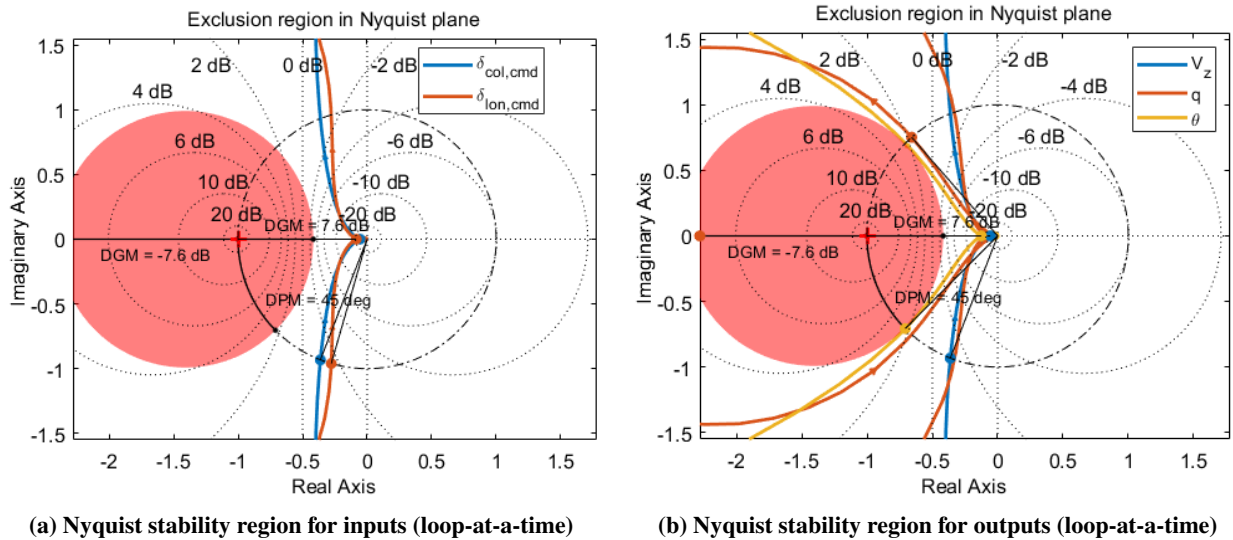


**Fig. 4** Nyquist plots with symmetric stability regions for the inputs/outputs (loop-at-a-time) of open loops for the design point at 40 kts

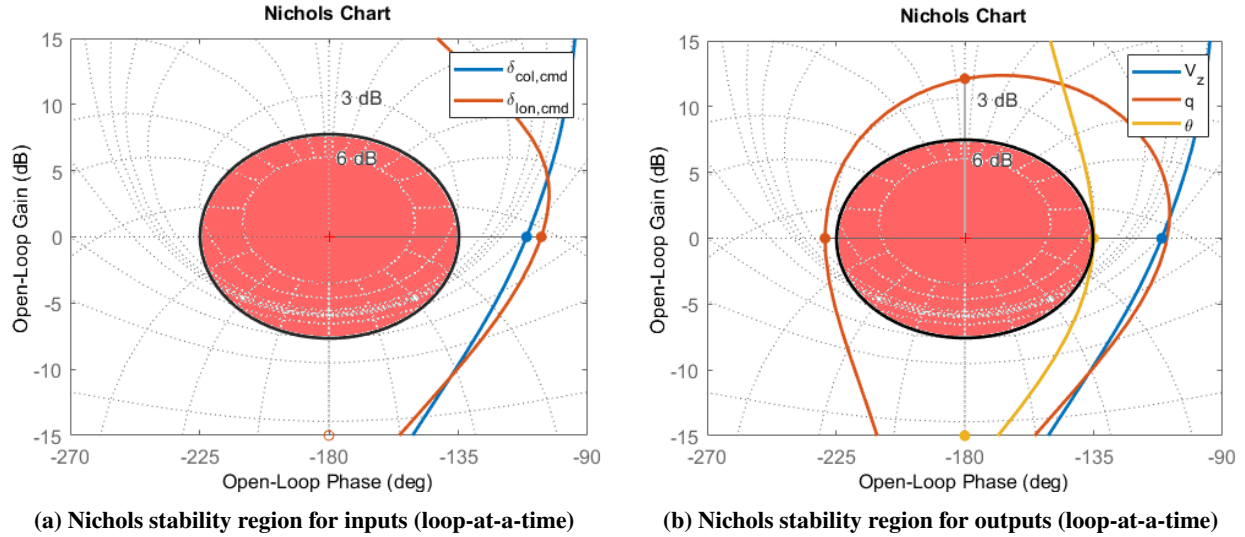


**Fig. 5** Nichols plots with symmetric stability regions for the inputs/outputs (loop-at-a-time) of open loops for the design point at 40 kts

As shown in the figure the exclusion regions are highlighted in which the broken open-loop transfer functions are avoided indicating robustness against perturbations for combinations of phase and gain margins, meeting the disk based stability requirements set. Additionally, Fig. (6) shows the hard requirement on the pole-location for  $\mathcal{D}$ -stability, ensuring that all poles in the closed-loop system are stable left-hand plane with sufficient damping in accordance with the HQ criteria. The same can be said for the zero locations which indicate minimum-phase behaviors and no RHP cancellations. Although, there are poles close to the marginal plane which have an impact the robustness of the controller design elaborated further in the analysis.

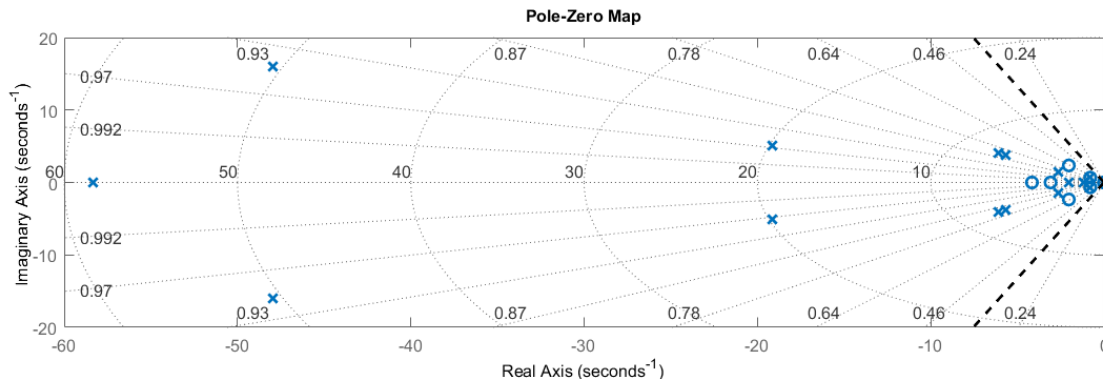
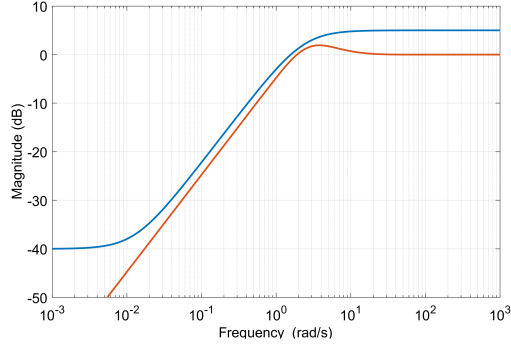


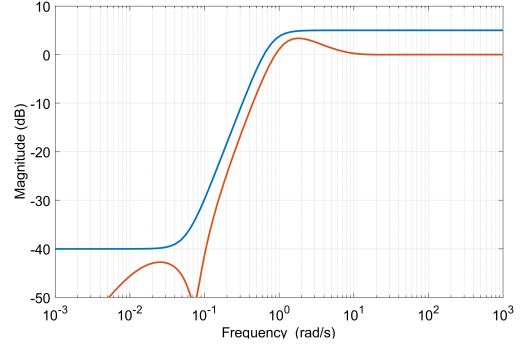
**Fig. 6** Closed-loop pole-zero plot for the design point at 40 kts

## B. Closed-loop Transfer Functions

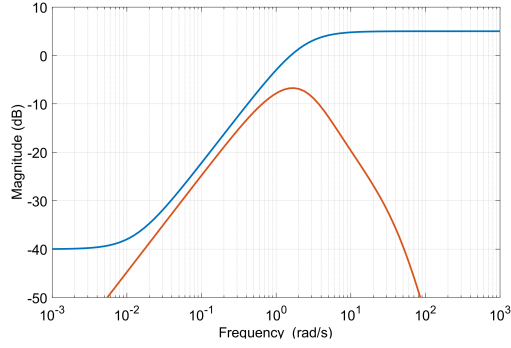
The five different closed-loop transfer functions that are constrained to assess the frequency-domain characteristics of the closed-loop system are shown in Fig. (7) for the 2-DoF controller. To attenuate I/O disturbances acting on both the plant input and output,  $S_o$  and  $S_o G$  signals are minimized at low frequencies. Furthermore, it can be seen that the  $K S_o$ ,  $T_i$  and  $T_o$  signals have adequate roll-off at high frequencies to attenuate the high frequency measurement noise.



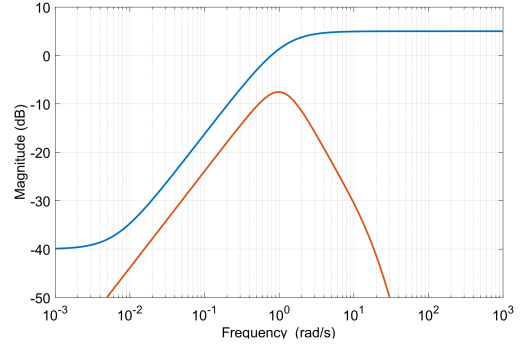
(a) Soft constraint on  $T_{d_{V_z} \rightarrow V_z}$  (output disturbance sensitivity on  $V_z$ )



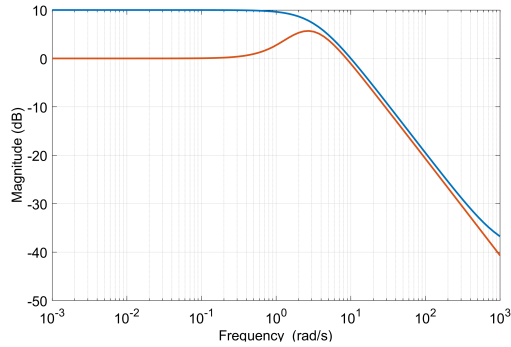
(b) Soft constraint on  $T_{d_{\theta} \rightarrow \theta}$  (output disturbance sensitivity on  $\theta$ )



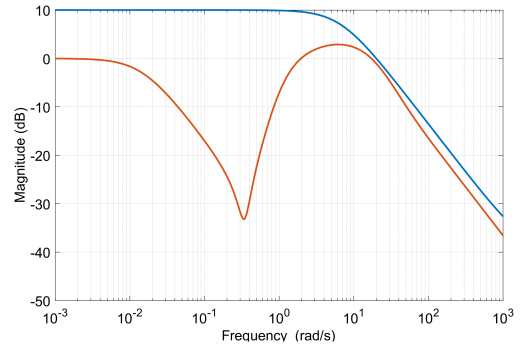
(c) Soft constraint on  $T_{d_{\delta_{col,cmd}} \rightarrow V_z}$  (input disturbance sensitivity on  $V_z$ )



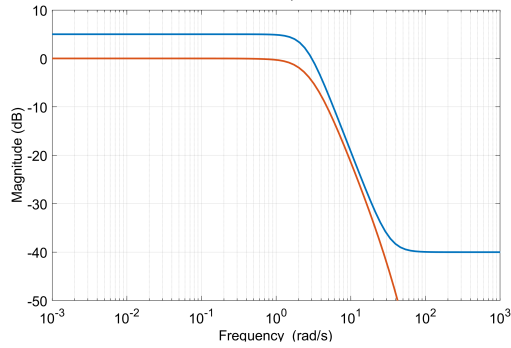
(d) Soft constraint on  $T_{d_{\delta_{lon,cmd}} \rightarrow \theta}$  (input disturbance sensitivity on  $\theta$ )



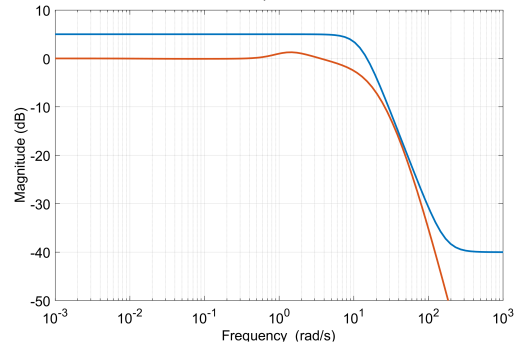
(e) Soft constraint on  $T_{d_{V_z} \rightarrow \delta_{col,cmd}}$  (output disturbance sensitivity on  $\delta_{col,cmd}$ )



(f) Soft constraint on  $T_{d_{\theta} \rightarrow \delta_{lon,cmd}}$  (output disturbance sensitivity on  $\delta_{lon,cmd}$ )



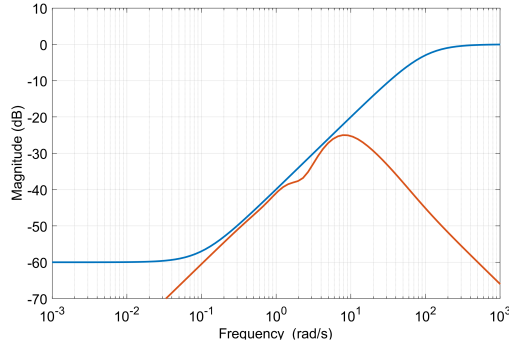
(g) Soft constraint on  $T_{d_{\delta_{col,cmd}} \rightarrow \delta_{col,cmd}}$  (input disturbance sensitivity on  $\delta_{col,cmd}$ )



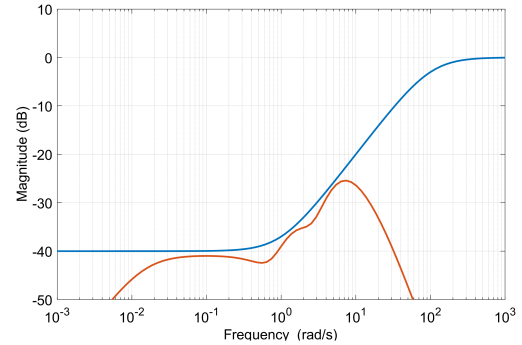
(h) Soft constraint on  $T_{d_{\delta_{lon,cmd}} \rightarrow \delta_{lon,cmd}}$  (input disturbance sensitivity on  $\delta_{lon,cmd}$ )

**Fig. 7** Overview of the designs of soft constraints related to disturbance rejection and signal attenuation frequency responses for the design point at 40 kts (blue: inverted weights  $W^{-1}$ , red: designed solution)

The closed-loop transfer functions of the 2-DoF controller design are shown in Fig. (8). It can be seen that  $T_o - T_{ref}$  has a high peak in the mid-frequency range and is low in the low-frequency which results in low steady-state error from sufficient integral action of the controller. This peak is reshaped with the feedforward controller, leading to the controlled system requiring more control effort in this frequency range without affecting the robustness of the feedback control. Furthermore, bounding the  $T_o - T_{ref}$  function in Fig. (8) to be small at lower frequencies will reduce the error between the reference model and the output of the system at lower to mid-frequencies. A trade-off takes place where the peak of  $T_o - T_{ref}$  is limited as much as possible in the mid-frequency range, while minimizing functions  $KS_o$  the required control effort in the from the reference tracking and  $T_i$  the input tracking so the signals have adequate roll-off at higher frequencies.



(a) Soft constraint on  $T_{V_{z_{ref}} \rightarrow V_z} - T_{ref, V_z}$  (reference tracking)



(b) Soft constraint on  $T_{\theta_{ref} \rightarrow \theta} - T_{ref, \theta}$  (reference tracking)

**Fig. 8 Overview of the designs of soft constraints related model following frequency responses for the design point at 40 kts (blue: inverted weights  $W^{-1}$ , red: designed solution)**

### C. Handling Quality Requirements

The performance of the resulting design is evaluated against the quickness and bandwidth of the attitude response which are the requirements that are enforced using a model following approach for the longitudinal helicopter model. The quickness criterion, defined by ADS-33, uses amplitude step inputs to assess the rate at which the controller converges to the target attitude while minimising overshoot using the peaks as metrics  $\frac{q_{pk}}{\theta_{pk}}$ . Fig. (9) shows the results obtained using the designed system in the time domain, which can be compared with the theoretical performance of the reference model. As can be seen, responses remain close to the targets defined by the reference models. This indicates that the combination of the reference model tracking approach leads to a consistent response of the flight control system solution in the time domain. Furthermore, the responses exhibit inter-axis decoupling between the channels, despite the absence of constraints directly associated with decoupling requirements. However, the risk of actuator saturation remains, which is a problem for the attitude quickness requirement. As shown in Fig. (9b), the attitude command quickness is  $\frac{q_{pk}}{\theta_{pk}} = 1.8 \text{ s}^{-1}$  meeting level 1 required for mission task elements (MTE) and attitude target acquisition ( $> 1.6 \text{ s}^{-1}$ ) requirement for 1 deg attitude changes.

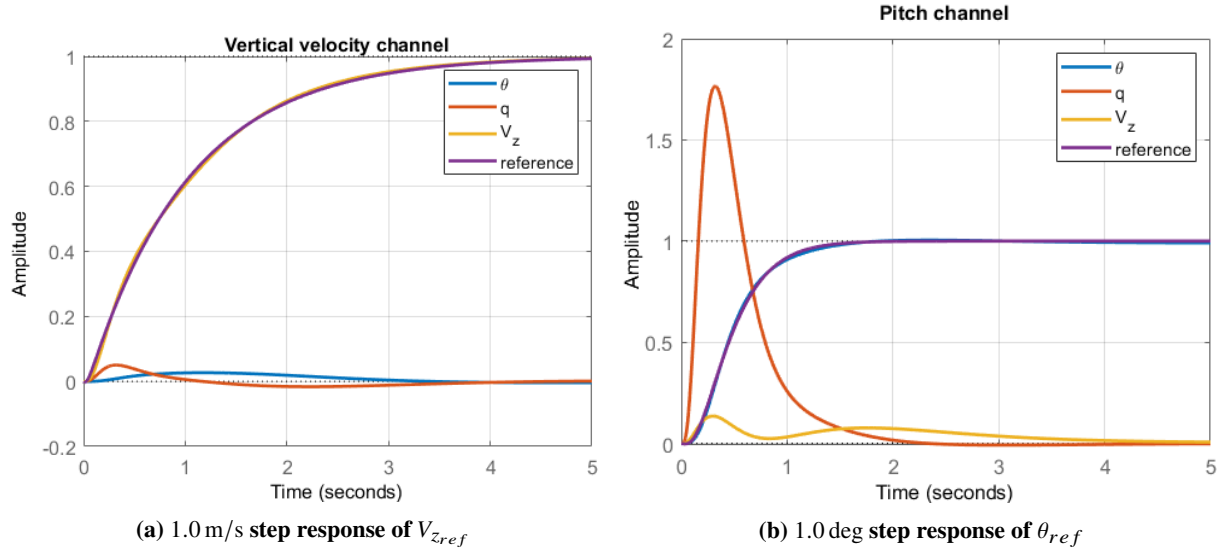


**Fig. 9 Step responses in the time domain**

The bandwidth handling criteria assess the accuracy of the reference tracking in the frequency domain using two parameters: the phase delay  $\tau_{p\theta}$  and bandwidth  $\omega_{BW\theta}$ . The bandwidth of the ACAH response types is the minimum between the frequency at which the phase is at  $-135$  deg and the frequency at which the gain is 6 dB greater than at the crossover frequency  $\omega_{180}$ . The phase delay  $\tau_{p\theta}$  is defined according to Eq. (24) in terms of the crossover frequency  $\omega_{180}$  and the phase shift at twice the crossover frequency  $\Delta\phi_{2\omega_{180}}$ . The application of this criterion to the designed flight control system from reference models is shown in Fig. (10), meeting level 1 handling requirements and closely matching the reference point [6].

$$\tau_{p\theta} = \frac{\Delta\phi_{2\omega_{180}}}{57.3(2\omega_{180})} \quad (24)$$

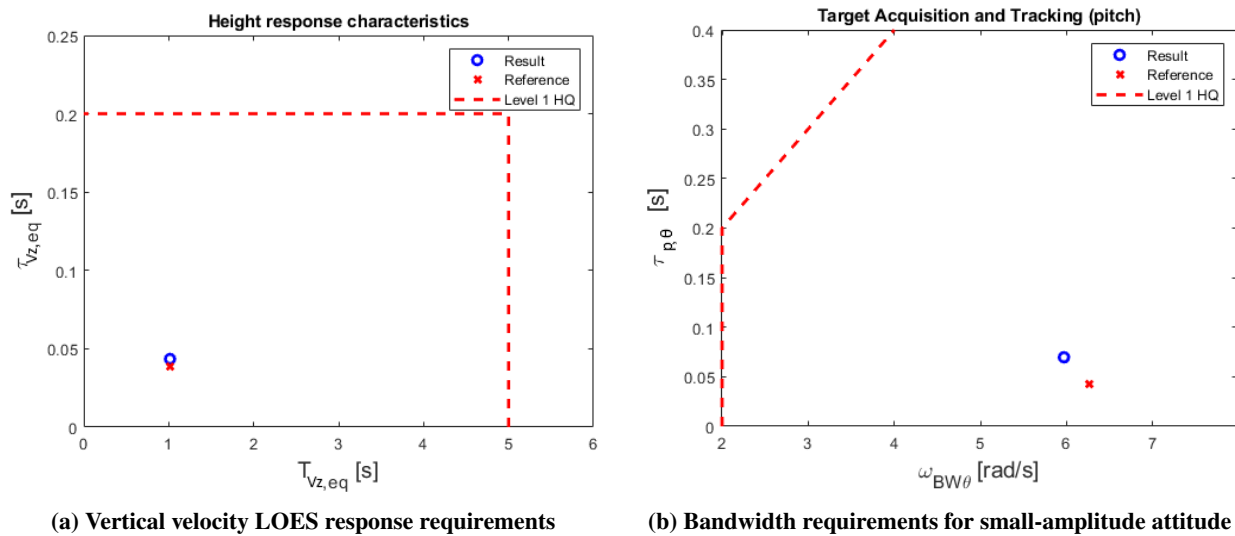


**Fig. 10 Model following frequency domain HQ requirement**

#### D. Robustness Analysis

To investigate robustness against uncertainties, an uncertain model of the helicopter was derived from the design model by defining a  $\pm 20\%$  uncertainty for all stability and control derivatives in matrices  $A$  and  $B$  of Eq. (1), with a breakdown of the uncertain derivatives with the most significant contributions. The robustness of the resulting controller is assessed using an SSV or  $\mu$  analysis, as shown in Fig. (11) [24].

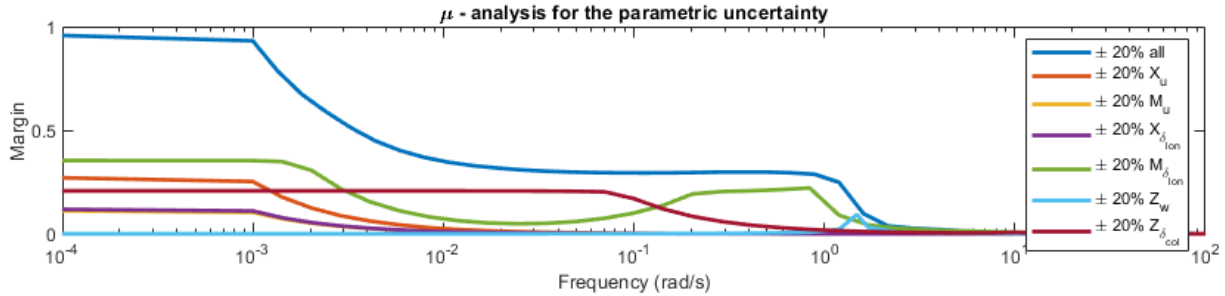


Fig. 11 Structured singular value analysis for the design point at 40 kts (stability and control derivatives)

The upper bound peak value is equal to 0.9988 at a critical frequency of 0 rad/s at the design velocity when all of the uncertainty is applied, indicating that robust stability for the uncertainty is guaranteed. This corresponds to the controller being capable of handling  $100/(0.9988) = 100.12\%$  of the uncertainty. Therefore, for values less than 1, the controller is robustly stable against the specified parametric uncertainty. The uncertainty in the longitudinal  $X$  and moment  $M$  derivatives significantly affect the phugoid dynamics, which are the major contributing factors towards the robustness limitations at 0 rad/s. In contrast, the normal  $Z$  derivatives affecting the heave subsidence, which is already stable in the open loop and has a less significant cumulative contribution to robust stability.

Furthermore, parametric uncertainties can be added directly into the nonlinear model using MATLAB's *ureal()* and linearized using *ulinearize()* to obtain an uncertain linear model for variations in mass and moment of inertia ( $m \pm 10\%$ ,  $I_{yy} \pm 10\%$ ) combined with variations in the center of gravity position both normally and longitudinally ( $Z_{CG}$ ,  $X_{CG} \pm 0.05$  m) from the nominal model. Additionally, multiplicative uncertainties in the aerodynamic forces and moments were added ( $F_x \pm 20\%$ ,  $F_z \pm 20\%$ ,  $M_y \pm 20\%$ ). This introduces uncertainties in the force/moment derivatives and operating points, which allows for the robustness of the resulting controller to be assessed at various flight configurations. The  $\mu$  analysis, shown in Fig. (12), demonstrating that the system is robustly stable against the parametric changes in the configuration and the uncertainty in the aerodynamic forces and moments, with a tolerance up to  $100/(0.238) = 420\%$ . This results shows that the controller is robustly stable against shifts in centre of gravity positions, uncertainty in the forces  $X$ ,  $Z$  and moment  $M$  as well as the changes in the mass and moment of inertia. This indicates that the limitation to the robustness of the autopilot are stability and control derivatives which significantly affect the phugoid dynamics of the helicopter.

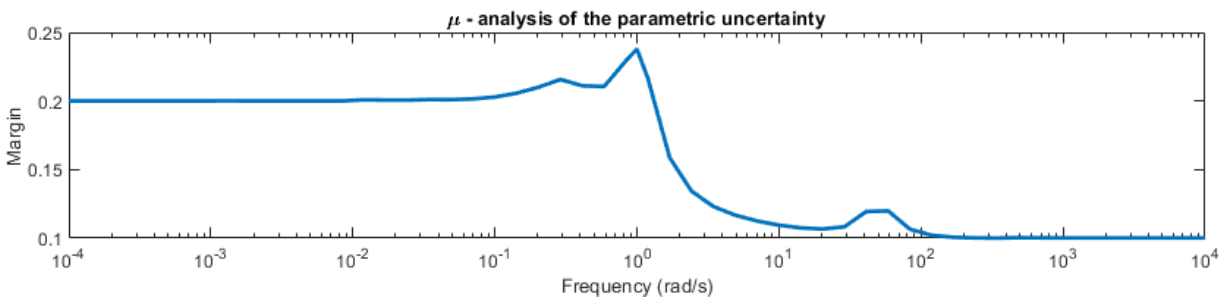


Fig. 12 Structured singular value analysis for the design point at 40 kts (configuration and forces/moments)

## VI. Non-linear simulations

To showcase the robustness of the controller, nonlinear Monte Carlo simulations were performed, as shown in Fig. (13), by varying uncertain parameters used for Fig. (12), which corresponds to the  $\mu$  analysis. The following simulations use a series of step-wise reference signals where the altitude is  $h = 0$  m to assess the non-linear performance. The reference signal profiles allow for flight coverage around the design point. In the simulation, uncertainties in the force/moment derivatives and operating points were introduced in the nonlinear 3-DoF longitudinal helicopter model. The commanded maneuvers were designed to stay within the limitations of actuators for the nominal model.

It can be seen that even for large vertical velocity changes and pitch angles, the control effort remains small, and the response accurately follows the reference signal. This is evident in the first 25 seconds, where the step functions were individually applied. Both steps converge to the reference signal; however, parametric uncertainty introduces notable variations in the vertical velocity response, particularly in terms of overshoot, while rise times remain consistent. Despite this, the ACAH response remains stable and consistent throughout the simulation, even under uncertainty.

Furthermore, while uncertainties influence the response, the controller is still able to accurately track the reference signal, albeit with some degradation in performance as uncertainty increases. This degradation is most evident in the vertical velocity control during simultaneous reference commands with the pitch channel for 5 deg steps. The steady-state error is approximately 0.1 m/s, which is relatively small. However, due to the non-linear coupling dynamics, greater variations occur in the final 30 seconds of the simulation for 15 deg step reference inputs.

To conclude, the simulation verified the results of the  $\mu$  analysis in the time domain, assuming that changes in the stability of the model are negligible as a function of velocity.

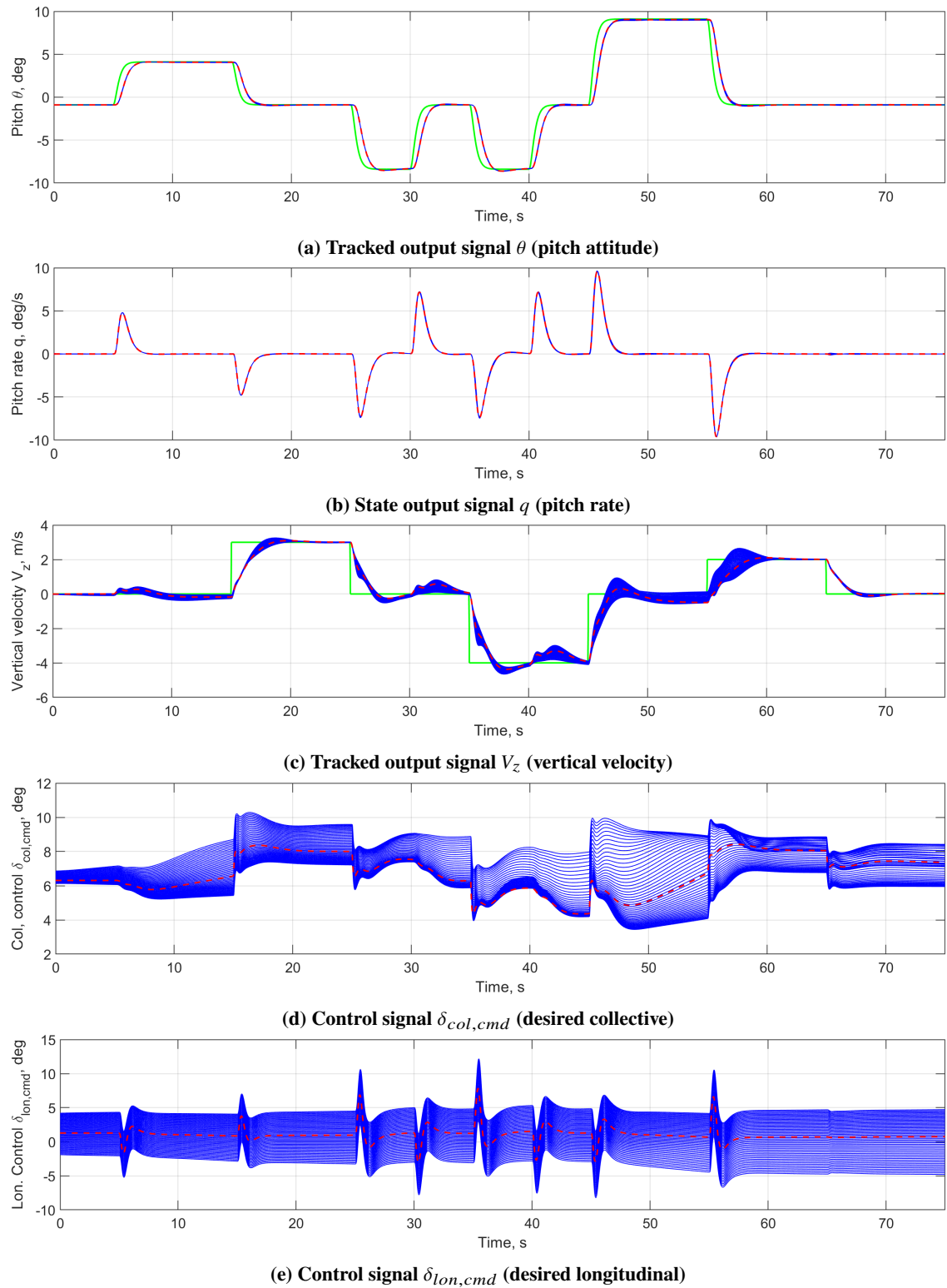


**Fig. 13** Nonlinear simulation (green: reference, red: nominal parameter run, blue: 50 uncertain parameter runs)

## VII. Conclusion

This paper introduced a flight control architecture combining robust control theory as a method for tuning controllers to meet HQ requirements. The design methodology adopts a multi-objective approach to balance trade-offs between robustness and performance in the controller design using the frequency domain. The proposed methodology uses simple structured controllers that can be gain-scheduled and/or applied in multi-modal methods to obtain robust controllers. Various soft and hard constraints were systematically applied, resulting in a 2-DoF longitudinal controller with desired properties for reference tracking, disturbance rejection at the plant inputs and outputs, sensor noise attenuation, control signal attenuation, and disk-based stability margins. Additionally,  $\mu$  analysis verified the robustness of the controller against various parametric uncertainties.

This methodology is limited by the designer's experience in handling the trade-offs between robustness and performance to meet HQ requirements and ensure the constraint parameters are properly tuned. Despite this limitation, the methodology simplifies the design process. Future work could focus on better understanding the connection between helicopter design limitations and control law design in terms of robustness and performance in meeting HQ requirements.

The next steps include testing the methodology on a higher fidelity nonlinear model of the helicopter to confirm the results obtained by applying the selected ADS-33 and stability criteria to the linear model. As a gain-scheduled controller and/or multi-model approaches can be used to account for nonlinear phenomena across the flight envelope. In addition, to development of the control architecture to take into account higher-order rotor dynamics, rotor flow state aerodynamics and aero-elasticity. Furthermore, robust control design under the constraints of actuator authority limits using anti-windup schemes also needs investigation.

## References

- [1] Padfield, G. D., *Helicopter flight dynamics: the theory and application of flying qualities and simulation modelling*, John Wiley & Sons, 2008.
- [2] Tischler, M. B., Berger, T., Ivler, C. M., Mansur, M. H., Cheung, K. K., and Soong, J. Y., *Practical methods for aircraft and rotorcraft flight control design: an optimization-based approach*, American Institute of Aeronautics and Astronautics, Inc., 2017.
- [3] Prouty, R. W., *Helicopter performance, stability, and control*, Krieger Pub., 1995.
- [4] Walker, D., "Multivariable control of the longitudinal and lateral dynamics of a fly-by-wire helicopter," *Control Engineering Practice*, Vol. 11, No. 7, 2003, pp. 781–795. [https://doi.org/https://doi.org/10.1016/S0967-0661\(02\)00189-2](https://doi.org/https://doi.org/10.1016/S0967-0661(02)00189-2), URL <https://www.sciencedirect.com/science/article/pii/S0967066102001892>.
- [5] Johnson, W., *Rotorcraft aeromechanics*, Vol. 36, Cambridge university press, 2013.
- [6] Anon, "ADS-33E-PRF-Handling Qualities Requirements for Military Rotorcraft," 2000. URL <https://www.robertheffley.com/docs/HQs/ADS-33E-PRF.pdf>.
- [7] Hu, J., and Gu, H., "Survey on Flight Control Technology for Large-Scale Helicopter," *International Journal of Aerospace Engineering*, Vol. 2017, No. 1, 2017. <https://doi.org/10.1155/2017/5309403>, URL <https://dx.doi.org/10.1155/2017/5309403>.
- [8] Anon, "Detailed specification: Flight systems—Design, installation, and test of piloted aircraft, general specification for MIL-DTL-9490E," 2008. URL [http://everyspec.com/MIL-SPECS/MIL-SPECS-MIL-DTL/MIL-DTL-9490E\\_10979/](http://everyspec.com/MIL-SPECS/MIL-SPECS-MIL-DTL/MIL-DTL-9490E_10979/).
- [9] Du Val, R. W., and He, C., "Validation of the FLIGHTLAB virtual engineering toolset," *The Aeronautical Journal*, Vol. 122, No. 1250, 2018, pp. 519–555. <https://doi.org/10.1017/aer.2018.12>, URL <https://dx.doi.org/10.1017/aer.2018.12>.
- [10] Balas, G. J., "Flight Control Law Design: An Industry Perspective," *European Journal of Control*, Vol. 9, No. 2, 2003, pp. 207–226. <https://doi.org/https://doi.org/10.3166/ejc.9.207-226>, URL <https://www.sciencedirect.com/science/article/pii/S0947358003702763>.
- [11] Kumar, M. V., Sampath, P., Suresh, S., Omkar, S., and Ganguli, R., "Design of a stability augmentation system for a helicopter using LQR control and ADS-33 handling qualities specifications," *Aircraft Engineering and Aerospace Technology*, Vol. 80, No. 2, 2008, pp. 111–123. <https://doi.org/10.1108/00022660810859337>.
- [12] Gribble, J. J., "Linear quadratic Gaussian/loop transfer recovery design for a helicopter in low-speed flight," *Journal of Guidance, Control, and Dynamics*, Vol. 16, No. 4, 1993, pp. 754–761. <https://doi.org/10.2514/3.21077>, URL <https://doi.org/10.2514/3.21077>.

- [13] Tijani, I. B., Akmeliawati, R., Legowo, A., Budiyo, A., and Abdul Muthalif, A. G., “ $\mathcal{H}_\infty$  Robust controller for autonomous helicopter hovering control,” *Aircraft Engineering and Aerospace Technology*, Vol. 83, No. 6, 2011, pp. 363–374. <https://doi.org/10.1108/00022661111173243>, URL <https://doi.org/10.1108/00022661111173243>.
- [14] Silva, L. R. T. d., Campos, V. A. F. d., and Potts, A. S., “Robust Control for Helicopters Performance Improvement: an LMI Approach,” *Journal of Aerospace Technology and Management*, Vol. 12, 2020. <https://doi.org/10.5028/jatm.v12.1179>.
- [15] Prempain, E., and Postlethwaite, I., “Static  $\mathcal{H}_\infty$  loop shaping control of a fly-by-wire helicopter,” *Automatica*, Vol. 41, No. 9, 2005, pp. 1517–1528. <https://doi.org/https://doi.org/10.1016/j.automatica.2005.04.001>, URL <https://www.sciencedirect.com/science/article/pii/S000510980500141X>.
- [16] Antonioli, J.-C., Taghizad, A., Rakotomamonjy, T., and Ouladsine, M., “Towards the development of a methodology for designing helicopter flight control laws by integrating handling qualities requirements from the first stage of tuning,” *40th European Rotorcraft Forum (ERF 2014)*, 2014. URL <https://hal.science/hal-01094364>.
- [17] Dai, J., Ying, J., and Tan, C., “A novel particle swarm optimization based robust H-infinity control for rotorcrafts,” *Engineering Computations*, Vol. 31, No. 4, 2014, pp. 726–741. <https://doi.org/10.1108/ec-07-2012-0148>, URL <https://dx.doi.org/10.1108/ec-07-2012-0148>.
- [18] Srinathkumar, S., “Eigenstructure Control: A Rotorcraft Handling Qualities Engineering Tool,” *Journal of the American Helicopter Society*, Vol. 60, No. 2, 2015, pp. 1–12. <https://doi.org/10.4050/JAHS.60.022010>.
- [19] Ji, S., and Wu, A., “Study on dual-loop controller of helicopter based on the robust H-infinite loop shaping and mixed sensitivity,” *2011 International Conference on Electrical and Control Engineering*, IEEE, 2011, pp. 1291–1294. <https://doi.org/10.1109/ICECENG.2011.6057783>.
- [20] Biannic, J.-M., Taghizad, A., Dujols, L., and Perozzi, G., “A multi-objective  $\mathcal{H}_\infty$  design framework for helicopter PID control tuning with handling qualities requirements,” *7th European Conference for Aeronautics and Space Science (EUCASS), Milan, Italy*, 2017, p. 89.
- [21] Authié, P., “A multi-model and multi-objective approach to the design of helicopter flight control laws,” *CEAS Aeronautical Journal*, Vol. 15, No. 3, 2024, pp. 529–543. <https://doi.org/10.1007/s13272-023-00675-w>.
- [22] Apkarian, P., and Noll, D., “Nonsmooth  $\mathcal{H}_\infty$  Synthesis,” *IEEE Transactions on Automatic Control*, Vol. 51, No. 1, 2006, pp. 71–86. <https://doi.org/10.1109/TAC.2005.860290>.
- [23] Skogestad, S., and Postlethwaite, I., *Multivariable feedback control: analysis and design*, John Wiley & sons, 2005.
- [24] Bates, D., and Postlethwaite, I., *Robust multivariable control of aerospace systems*, Vol. 8, IOS Press, 2002.
- [25] P. Apkarian, D. N., “The  $\mathcal{H}_\infty$  Control Problem is Solved,” *AerospaceLab*, , No. 13, 2017. <https://doi.org/10.12762/2017.al13-01>, URL <https://dx.doi.org/10.12762/2017.al13-01>.
- [26] “Robust controller order reduction,” *International Journal of Control*, Vol. 84, No. 5, 2011, pp. 985–997. <https://doi.org/10.1080/00207179.2011.585474>, URL <https://doi.org/10.1080/00207179.2011.585474>.
- [27] Theodoulis, S., and Proff, M., *Robust Flight Control Tuning for Highly Agile Missiles*, 2021. <https://doi.org/10.2514/6.2021-1568>, URL <https://arc.aiaa.org/doi/abs/10.2514/6.2021-1568>.
- [28] Srinathkumar, S., “Rotorcraft Precision Hover Control in Atmospheric Turbulence via Eigenstructure Assignment,” *Journal of the American Helicopter Society*, Vol. 64, No. 1, 2019, pp. 1–12. <https://doi.org/10.4050/JAHS.64.012005>, URL <https://www.ingentaconnect.com/content/ahs/jahs/2019/00000064/00000001/art00005https://doi.org/10.4050/JAHS.64.012005>.
- [29] Pavel, M. D., *Six degrees of freedom linear model for helicopter trim and stability calculation*, Delft University of Technology, Faculty of Aerospace Engineering, 1996.
- [30] Simplicio, P., Pavel, M., van Kampen, E., and Chu, Q., “An acceleration measurements-based approach for helicopter nonlinear flight control using Incremental Nonlinear Dynamic Inversion,” *Control Engineering Practice*, Vol. 21, No. 8, 2013, pp. 1065–1077. <https://doi.org/https://doi.org/10.1016/j.conengprac.2013.03.009>, URL <https://www.sciencedirect.com/science/article/pii/S0967066113000634>.
- [31] Vicente Melo E Carvalho Marques, M., “Investigation of L1 Adaptive Control as an Augmentation Loop,” Master’s thesis, Delft University of Technology, 2017.

- [32] Bouwer, G., and Hilbert, K. B., "A Piloted Simulation of a Model Following Control System," *Journal of the American Helicopter Society*, Vol. 31, No. 2, 1986, pp. 27–32. <https://doi.org/10.4050/JAHS.31.2.27>, URL <https://www.ingentaconnect.com/content/ahs/jahs/1986/00000031/00000002/art00004>.
- [33] Apkarian, P., and Noll, D., "Nonsmooth optimization for multiband frequency domain control design," *Automatica*, Vol. 43, No. 4, 2007, pp. 724–731. <https://doi.org/https://doi.org/10.1016/j.automatica.2006.08.031>, URL <https://www.sciencedirect.com/science/article/pii/S0005109806004559>.
- [34] Seiler, P., Packard, A., and Gahinet, P., "An Introduction to Disk Margins [Lecture Notes]," *IEEE Control Systems Magazine*, Vol. 40, No. 5, 2020, pp. 78–95. <https://doi.org/10.1109/MCS.2020.3005277>.
- [35] Chilali, M., Gahinet, P., and Apkarian, P., "Robust pole placement in LMI regions," *IEEE Transactions on Automatic Control*, Vol. 44, No. 12, Apkarian, P., pp. 2257–2270. <https://doi.org/10.1109/9.811208>.
- [36] Berger, T., Ivler, C., Berrios, M. G., Tischler, M. B., and Miller, D., "Disturbance rejection handling qualities criteria for rotorcraft," *72nd Annual Forum of the American Helicopter Society, West Palm Beach, USA*, 2016. <https://doi.org/10.4050/F-0072-2016-11452>.
- [37] Apkarian, P., "Tuning controllers against multiple design requirements," *2013 American Control Conference*, 2013, pp. 3888–3893. <https://doi.org/10.1109/ACC.2013.6580433>.
- [38] Apkarian, P., Gahinet, P., and Buhr, C., "Multi-model, multi-objective tuning of fixed-structure controllers," *2014 European Control Conference (ECC)*, 2014, pp. 856–861. <https://doi.org/10.1109/ECC.2014.6862200>.